

# 850 nm Vertical-Cavity Surface-Emitting Laser Arrays With Enhanced High-Speed Transmission Performance Over a Standard Multimode Fiber

Jia-Liang Yen, Xin-Nan Chen, Kai-Lun Chi, Jason Chen, and Jin-Wei Shi, *Senior Member, IEEE*

**Abstract**—The functionality of novel parallel and series high-speed vertical-cavity surface-emitting laser (VCSEL) arrays, which can greatly relax the tradeoff between output power and modulation speed, is demonstrated. Both types of array structure allow improvement in the output power with no degradation in their maximum modulation speed as compared to a single reference unit. The observed invariant electrical–optical bandwidth shown for these array structures is mainly due to the effective reduction of the differential resistance and parasitic capacitance, arising from the Zn-diffusion and oxide-relief apertures fabricated in the VCSEL unit. This in turn minimizes the degradation in the RC-limited bandwidth with the VCSEL arrays. Furthermore, the dense packing of single VCSELs, with Zn-diffusion apertures for optical mode control, minimizes the coupling loss between the output from the array into a standard multimode fiber (MMF). Compared with the single VCSEL unit, the parallel VCSEL array shows a significant enhancement in transmission performance over a standard OM4 MMF, which includes a larger eye margin, a higher signal-to-noise ratio, as well as a higher error-free data rate (48 versus 44 Gbit/sec). The device modeling technique is used to perform device analysis. From the results we can conclude that the improvement with the parallel array is because the value of the internal impedance is closer to the 50- $\Omega$  signal source, which minimizes the microwave reflection induced timing jitter in the eye-patterns.

**Index Terms**—Optical interconnects, semiconductor lasers, vertical cavity surface emitting lasers.

## I. INTRODUCTION

**V**ERTICAL-CAVITY surface-emitting lasers (VCSELs) with central wavelengths of 850 nm have become the most

Manuscript received September 3, 2016; revised December 2, 2016 and January 18, 2017; accepted March 5, 2017. Date of publication March 6, 2017; date of current version June 24, 2017. This work was supported by the Ministry of Science and Technology in Taiwan under Grants MOST 104-2218-E-008-004 and MOST 103-2622-E-009-004-CC2.

J.-L. Yen is with the Department of Information Technology, Tainan University of Science and Technology, Taipei 114, Taiwan (e-mail: iamthats@gmail.com).

X.-N. Chen and K.-L. Chi are with the Department of Electrical Engineering, National Central University, Taoyuan 320, Taiwan (e-mail: s30642@gmail.com; porpoise5233@msn.com).

J. Chen is with the Department of Photonics, National Chiao-Tung University, Hsinchu 300, Taiwan (e-mail: jchen@mail.nctu.edu.tw).

J.-W. Shi is with the Department of Electrical and Computer Engineering, University of California Santa Barbara, Santa Barbara, CA 93106 USA, on leave from the Department of Electrical Engineering, National Central University, Taoyuan 320, Taiwan (e-mail: jwshi@ee.ncu.edu.tw).

Color versions of one or more of the figures in this paper are available online at <http://ieeexplore.ieee.org>.

Digital Object Identifier 10.1109/JLT.2017.2679200

important light source in the booming market of short-reach (< 300 meters) optical interconnects (OI) [1]–[5]. The target for the next generation interconnect framework is a data rate per channel of 56 Gbit/sec (CEI (Common Electrical Interface)-56G) [1]–[5] with a total data rate of up to 400 Gbit/sec. Complex modulation/de-modulation techniques, such as pulse-amplitude modulation (PAM) [6], orthogonal frequency-division multiplexing (OFDM) [7], [8], and feed forward equalization (FFE) [5], [9] have been demonstrated to alleviate the speed bottleneck for an 850 nm VCSEL under direct modulation. However, the use of the afore-mentioned techniques to boost the data rate makes the power budget in the linking channel even more critical. The designing of VCSELs which simultaneously offer high modulation-speeds, high slope-efficiency, and enough output power, is thus very important to meet the requirements of the next-generation OI. In addition, high-speed VCSELs usually have a differential resistance of over 100  $\Omega$  [1], which is twice that of the typical 50  $\Omega$  high-speed laser driver used for data transmission. Such an impedance mismatch between the light source and driving circuit can lead to even more serious degradation in the quality of the transmitted eye-patterns when the data rate is further increased [10], [11]. The operation of several VCSELs in parallel as a high-power and high-speed VCSEL array [12] is one of the most promising solutions to further increase the total output power while reducing device resistance during high-speed modulation. However, degradation in the modulation speed of a parallel VCSEL structure as compared to that of a single unit is usually observed, due to the increase in the parasitic capacitance of the VCSEL array [12]. The creation of several light-emitters in a series (cascade) using single or individual optical resonators is an attractive solution to overcome the afore-mentioned trade-off between speed and output power. This approach has been successfully implemented using edge-emitting lasers [13], VCSELs, [14] and light-emitting diode (LEDs) [15]. It is found that the differential quantum efficiency (output power) is linearly proportional to the number of light-emitters in the series without sacrifice of the modulation speed as compared to that of a single reference device [15].

However, regardless of whether for a series or a parallel VCSEL array [12], [14], [16], it is usually necessary to use a bundle of MMFs or a multi-core MMF to combine the output power from the array, which can significantly increase the cost of the device package. In this study, we demonstrate novel densely

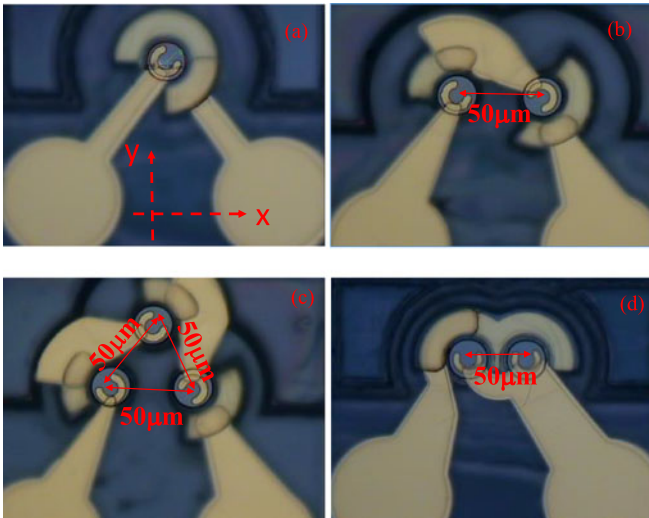


Fig. 1. Top-view of the demonstrated VCSELs: (a) single-unit, (b) two-unit series array, (c) three-unit series array, and (d) two-unit parallel array.

packed VCSEL array structures [17] with parallel and series connections. This design can greatly relax the trade-off between the modulation speed and maximum output power, and allow a reasonable coupling efficiency with a single-core MMF. The use of VCSEL units with Zn-diffusion and oxide-relief apertures [5], [11] can significantly reduce the differential resistance and parasitic capacitance, respectively. This in turn leads to the invariant high-speed performance of our demonstrated series and parallel arrays compared to that of a single unit reference sample. Furthermore, thanks to the good mode controllability of the Zn-diffusion apertures in our VCSEL units, the measured far-field patterns of the array are close to those measured for the single unit device, thereby avoiding any further increase in the coupling loss between the output light and the multi-mode fiber (MMF). Compared to the series array and the single device, the parallel array shows the best high-speed data transmission performance through an OM4 MMF. The measured microwave scattering (S) parameters show that this is because the parallel array has an impedance value closer to that of the 50  $\Omega$  signal source, which minimizes undesired microwave reflection induced jitter/noise in the measured eye-patterns. In comparison with the reference VCSEL unit, the two-unit parallel array shows a two-fold improvement in the maximum output power (8 vs. 4 mW), with the same 3-dB electrical-to-optical (E-O) bandwidth ( $\sim 25$  GHz), and enhancement of the maximum error-free data rate (48 vs. 44 GHz) via 2 meter OM4 MMF transmission.

## II. DESIGN OF DEVICE STRUCTURE AND FABRICATION

Fig. 1(a) to (d) show top-views of the demonstrated single reference VCSEL, two-unit and three-unit series VCSEL arrays, and two-unit parallel VCSEL array, respectively. For a conceptual cross-sectional view of the unit VCSEL please see our previous work [5], [11]. In early work on 850 nm VCSELs, the differential resistance was usually found to be limited by the p-type distributed-Bragg-reflectors (DBRs). Both graded bandgap layers (GBLs) [18] and Zn-diffusion [19] structures have been

demonstrated to overcome this problem. The addition of Zn-diffusion apertures in the top p-type DBR layers of our VCSEL, allows us not only to reduce the differential resistance of the device but can also manipulate the number of optical transverse modes inside the VCSEL cavity [5], [11], [20]. Combining these Zn-diffusion structures and an advanced GBL growth technique we produce 850 nm VCSELs with high single-mode (SM), high-speed, and low differential resistance ( $\sim 50 \Omega$ ) performance [20], close to the impedance of the driving circuit. However, there is significant intra-cavity loss induced by the Zn-diffusion apertures for SM performance, leading to an increase in the threshold gain (current), and the 3-dB E-O bandwidth is usually limited to around 12 GHz. To attain the ultimate high-speed performance ( $\sim 27$  GHz 3-dB E-O bandwidth) [1], [3], [5], [10] of the VCSEL and to extend the maximum linking distance through an OM4 fiber, miniaturized oxide-apertures (3-4  $\mu\text{m}$ ) offering nearly SM performance are still necessary [1], [3], [10] which would lead to a differential resistance as high as 200  $\Omega$ . However, there is a significant impedance-mismatch between the VCSEL and the 50  $\Omega$  driving signal source which produces undesired microwave reflections and degradation in the eye-patterns during high-speed data transmission [10]. In contrast, our Zn-diffusion VCSELs [5] demonstrate a close 3-dB bandwidth ( $\sim 27$  GHz) and the size of the oxide-apertures ( $\sim 3 \mu\text{m}$ ) lead to smaller values of differential resistance ( $< 100 \Omega$  vs. 200  $\Omega$ ). Although this value is still too high to match the 50  $\Omega$  driving source, the parallel array structure can be used to overcome the problem (as discussed below). An increase in total device capacitance and degradation in the RC-limited bandwidth are common problems with parallel arrays [12]. Here, the adoption of the oxide-relief structure in our VCSEL greatly minimizes the parasitic capacitance of the array [5], [11]. This is the key to sustaining an invariant net E-O bandwidth in the parallel array, as compared to that of the single reference unit. Details about dynamic measurement will be discussed later. The diameters of the Zn-diffusion ( $W_z$ ) and oxide-relief apertures ( $W_o$ ) and the Zn-diffusion depths ( $d$ ) of the measured devices are specified in the captions to the figures below. The epi-layer structure, purchased from LandMark<sup>1</sup>, is grown on a semi-insulating GaAs substrate, which is composed of three  $\text{In}_{0.1}\text{Ga}_{0.9}\text{As}/\text{Al}_{0.3}\text{Ga}_{0.7}\text{As}$  (40/80  $\text{\AA}$ ) MQWs sandwiched between 36-pair n-type and 26-pair p-type  $\text{Al}_{0.9}\text{Ga}_{0.1}\text{As}/\text{Al}_{0.12}\text{Ga}_{0.88}\text{As}$  Distributed-Bragg-Reflector (DBR) layers with an  $\text{Al}_{0.98}\text{Ga}_{0.02}\text{As}$  layer (50 nm thick) above the MQWs for oxidation. Fabry-Perot (FP) dip mapping of the whole VCSEL wafer shows that the cavity resonant wavelength is located at around 860 nm and that detuning between the gain peak (839 nm) and FP dip ( $\sim 860$  nm) wavelengths can be as large as around 20 nm. Such strong detuning will result in significant improvement in the 3-dB O-E bandwidth of the VCSEL due to the device self-heating induced red-shift of the gain peak under high bias currents [11].

To realize the series array, as shown in Fig. 1(b) and (c), each unit device (with a  $\sim 23 \mu\text{m}$  diameter active mesa) is etched down to the semi-insulation GaAs substrate for electrical isolation. Metal interconnects bridge the p- and n-contacts of neighboring devices for series connection. The device units in the parallel array share the same n-type metal contacts for parallel

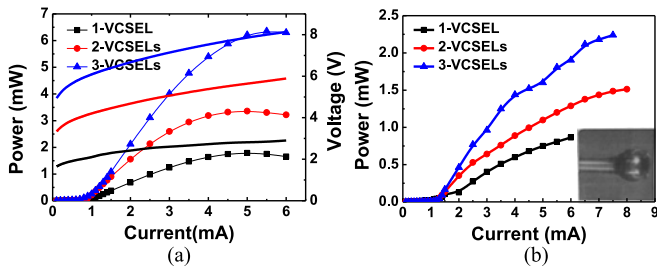


Fig. 2. (a) Measured L-I-V curves of the series arrays with different numbers of unit devices and their free-space output power. (b) Coupled power from the array into a single OM4 MMF. The inserted figure shows the tip of the fiber used for the collection of light ( $W_z/W_o/d = 8/3.5/1 \mu\text{m}$ ).

connections, as shown in Fig. 1(d). For collection of the output light over an MMF with a  $50 \mu\text{m}$  core diameter, the centers of neighboring light-emission apertures in the array should be set as close as possible, around  $50 \mu\text{m}$  apart. The slot line pads are integrated into the arrays or single reference unit for on-wafer high-speed measurement. For details of the fabrication process please refer to our previous work [11].

### III. MEASUREMENT RESULTS

The free-space light output power and bias voltages versus current (L-I and V-I) characteristics of the single unit reference device, and two-unit, and three-unit series arrays are shown in Fig. 2(a). As can be seen, the differential quantum efficiency, turn-on voltage, differential resistance, and maximum output power are all linearly proportional to the number of cascaded units in the array. Thanks to the Zn-diffusion apertures in these arrays, the differential resistances of the single, two- and three-unit arrays under the same 5 mA bias current can be as low as 78, 167, and 278  $\Omega$ , respectively. These resistance values are much smaller than those reported for a single high-speedbrk 850 nm VCSEL whose  $W_o$  is close in value to ours at  $\sim 3 \mu\text{m}$  [1]. Fig. 2(b) shows the power coupling characteristics into an MMF versus current for the single unit reference device, and the two-, and three-unit arrays. The inset shows a photograph of the tip of the MMF used for light collection. The size and shape of the ball-lens on the tip of the MMF were optimized to collect as much of the output light from the array as possible. The coupling efficiencies of the single unit and three-unit arrays are around 35 and 30% that of the free-space measurement result, respectively. The closeness in the values of the coupling efficiency suggest that the far-field patterns of the single unit and three-unit series array will be very similar, which will be discussed later.

Fig. 3(a) shows the measured free-space light output power and bias voltages versus current (L-I and V-I) characteristics of our single unit device and the two-unit parallel array. The diameter of the current confined aperture ( $W_o$ ) is around  $4.5 \mu\text{m}$ . We can clearly see that the free-space maximum output power (8 vs. 4 mW) and threshold current (1.6 vs. 1 mA) of the two-unit array are both about twice that of the single unit reference. Furthermore, the measured differential resistance of the parallel array is around half that of the single unit device (38 vs. 57  $\Omega$  at 15 and 8 mA, respectively.). These L-I-V measurement results suggest a nearly uniform current distribution in our

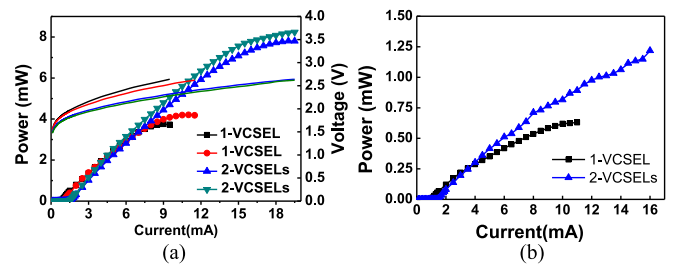


Fig. 3. (a) Measured L-I-V curves of parallel arrays with different numbers of unit devices and the free-space output power. (b) Coupled power from the array into a single OM4 MMF ( $W_z/W_o/d = 8/4.5/1 \mu\text{m}$ ).

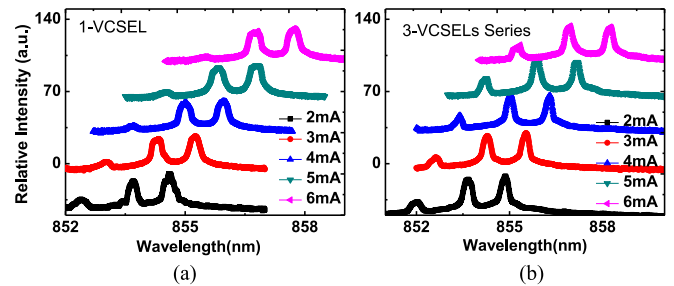


Fig. 4. Measured output optical spectra under different bias currents for the (a) single VCSEL and (b) 3-unit series array ( $W_z/W_o/d = 8/3.5/1 \mu\text{m}$ ).

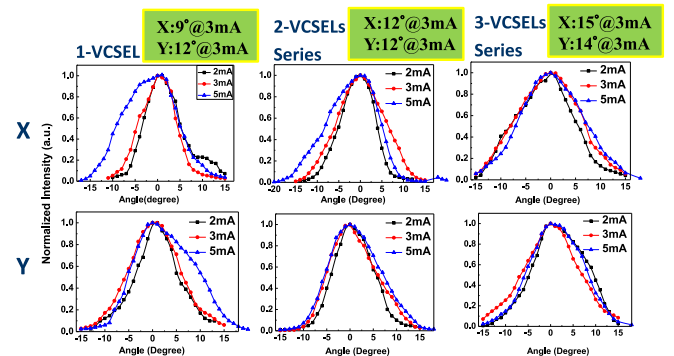


Fig. 5. Measured 1-D far-field patterns (X- and Y- directions) of the single VCSEL, and 2-unit, and 3-unit series arrays under different bias currents ( $W_z/W_o/d = 8/3.5/1 \mu\text{m}$ ).

two-unit parallel array. Fig. 3(b) shows the coupled power vs. bias current from our single unit device and 2-unit parallel array into a single MMF tip. The lower coupling efficiency ( $\sim 30$  vs.  $\sim 15\%$ ) of the parallel array as compared to that of the series array is mainly due to the larger divergence angle of the far-field patterns. This is because the parallel array has a larger size of  $W_o$  than that of the series array (4.5 vs.  $3.5 \mu\text{m}$ ), which induces more optical modes in its output spectrum and broadens the far-field patterns.

Fig. 4(a) and (b) show the measured output optical spectra of the single device and the three-unit series array. Thanks to the Zn-diffusion process, which can stabilize the output optical spectra, the quasi single-mode output performance of both devices is similar.

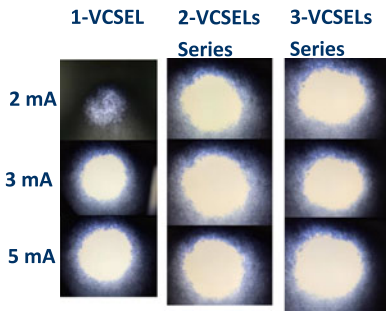


Fig. 6. Measured 2-D far-field patterns of the single VCSEL, and the 2 and 3-unit series arrays under different bias currents ( $W_z/W_o/d = 8/3.5/1 \mu\text{m}$ ).

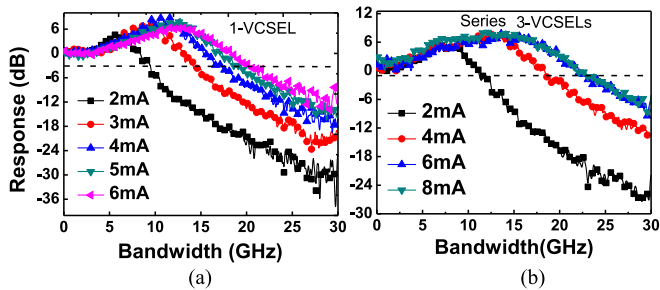


Fig. 7. Measured E-O frequency responses of the (a) single device and (b) 3-unit series array under different bias currents ( $W_z/W_o/d = 8/3.5/1 \mu\text{m}$ ).

Figs. 5 and 6 show the corresponding 1-dimensional (1-D) and 2-D far-field patterns of the single unit, two-unit, and three-unit series arrays under different bias currents. The  $x$ - and  $y$ -directions are defined in Fig. 1. It can be clearly seen that the far-field divergence angle ( $\sim 12^\circ$ ) and circular patterns of all three devices are very similar under the same bias current. This measurement result confirms that the coupling efficiency (from the device to MMF) of both the single unit and three series arrays are in reality very close in value (35 vs. 30%) as shown in Fig. 2(b). In contrast to the series array, the parallel array shows an MM behavior due to the larger sized oxide-relief apertures (3.5 vs.  $4.5 \mu\text{m}$ ). Nevertheless, the measured output optical spectra and far-field divergence angles of our single and two-unit parallel arrays are still very similar. The far-field divergence angles ( $\sim 17^\circ$ ) under bias currents of 3 mA (single unit) and 6 mA (two-unit) are very close. The broad divergence angle of the parallel array (12 vs.  $17^\circ$ ) results in a higher coupling loss than that of the series array, as can be seen in Figs. 2 and 3.

The high-speed E-O performance of the fabricated devices was measured by a lightwave component analyzer (LCA), which was composed of a network analyzer (Anritsu 37397C) and a calibrated 25 GHz photoreceiver module (New Focus 1481-S). Figs. 7 and 8 show the typical measured bias dependent E-O frequency responses for the series and parallel arrays, respectively. We can clearly see that, regardless of the kind of array, there is no degradation in the measured E-O bandwidth with an increase in the number of device units included. There is even a slight increase in the maximum 3-dB O-E bandwidth for the three-unit array, from 21 to 23 GHz, as compared to that of the single reference unit. Fig. 9(a) and (b) summarize the 3-dB O-E

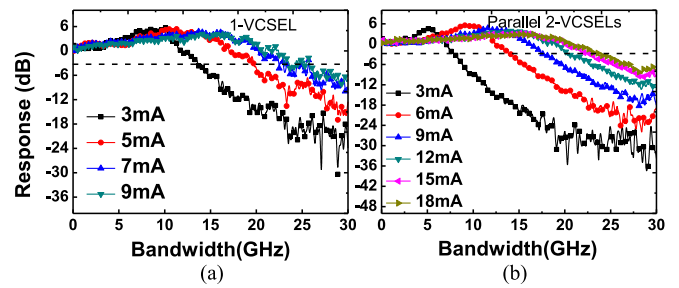


Fig. 8. Measured E-O frequency responses of the (a) single unit device and (b) 2-unit parallel array under different bias currents ( $W_z/W_o/d = 8/4.5/1 \mu\text{m}$ ).

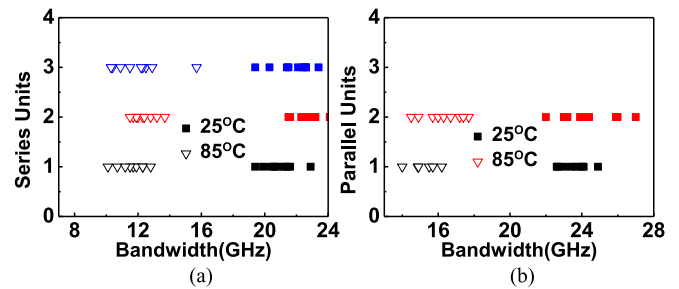


Fig. 9. Measured E-O 3-dB bandwidths of the (a) series array ( $W_z/W_o/d = 8/3.5/1 \mu\text{m}$ ) and (b) parallel array ( $W_z/W_o/d = 8/4.5/1 \mu\text{m}$ ) with different numbers of unit device inside at RT and under  $85^\circ\text{C}$  operation.

bandwidths (at RT and  $85^\circ\text{C}$ ) for the parallel and series arrays, respectively. The measurement results for several devices are specified in each figure. The distribution in the speed performance between devices is mainly due to variation in the process of mesa wet etching and oxidation of the oxide-apertures. As can be seen, the parallel array shows less degradation in speed compared to that of the series array ( $\sim 24$ -16 GHz vs.  $\sim 22$ -12 GHz) when the ambient temperature reaches  $85^\circ\text{C}$ . This can be attributed to the much smaller differential resistance of the parallel array than that of the series array; see Figs. 2 and 3 [11].

In most cases, there is significant degradation in the bandwidths of the parallel and series arrays compared to that of a single device, due to the increase in parasitic capacitance and differential resistance. However, this is not the case with our dynamic measurement results as discussed above. The device modeling technique is performed in order to investigate the invariant high-speed performance of our arrays and find their RC-limited bandwidth [21]. Fig. 10 shows the measured bias dependent microwave reflection coefficients ( $S_{11}$ ) of the series/parallel arrays and the single reference unit. Compared to the single unit reference device, the measured  $S_{11}$  trace of the series array moves closer to the open circuit point on the Smith Chart. This is because the differential resistance (impedance) of the series array increases with the number of units in the array.

This high value of the device impedance will induce significant microwave reflections between the device and the  $50 \Omega$  driving circuits, leading to degradation of the eye-patterns during high-speed data transmission. This will be discussed later. In

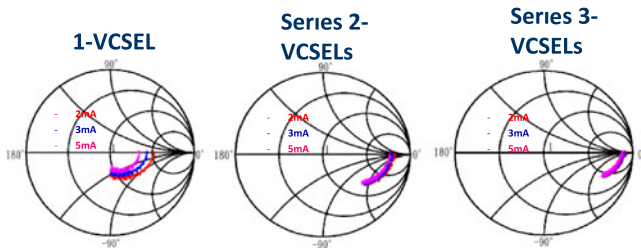


Fig. 10. Measured microwave reflection scattering ( $S_{11}$ ) parameters plotted on a Smith Chart for the single unit device, and 2-unit and 3-unit series arrays under different bias currents ( $W_z/W_o/d = 8/3.5/1 \mu\text{m}$ ).

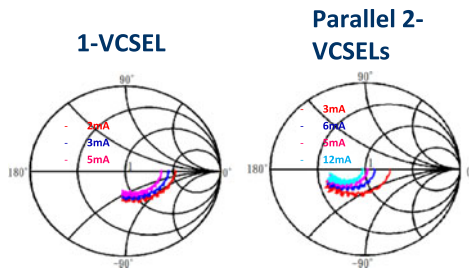


Fig. 11. Measured microwave reflection scattering ( $S_{11}$ ) parameters plotted on a Smith Chart of the single unit device and 2-unit parallel array under different bias currents ( $W_z/W_o/d = 8/4.5/1 \mu\text{m}$ ).

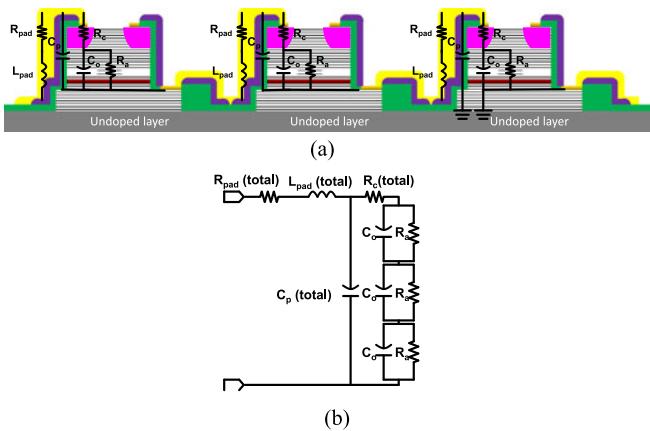


Fig. 12. (a) Conceptual cross-sectional and corresponding equivalent circuit model of a series VCSEL array. (b) Schematic representation of the equivalent circuit model.

contrast to the series array and the single unit reference device, the measured  $S_{11}$  trace of the parallel arrays moves closer to the center of the Smith chart, which represents the  $50 \Omega$  internal impedance of the device. The impedance-mismatch induced microwave reflections of the single device and the series array can thus be minimized. From the measured  $S_{11}$  parameters and using the equivalent-circuit modeling technique, we further extract the RC-limited bandwidths of our arrays and the single unit device [21].

Fig. 12 (a) and (b) show conceptual cross-sectional views of the series array and its equivalent-circuit model. Here,  $R_c$  is the contact resistance of the array;  $C_o$  is the parasitic

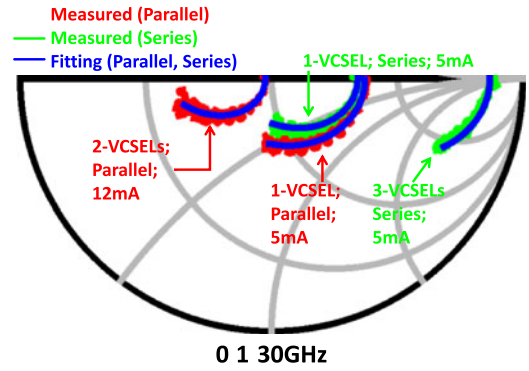


Fig. 13. Measured and fitted  $S_{11}$  parameters for the single unit (at 5 mA), 3-unit series ( $W_z/W_o/d = 8/3.5/1 \mu\text{m}$ ; at 5 mA), and 2-unit parallel array ( $W_z/W_o/d = 8/4.5/1 \mu\text{m}$ ; at 12 mA) plotted on a Smith Chart.

TABLE I  
VALUES OF THE CIRCUIT ELEMENTS USED FOR THE FITTING PROCESSES  
( $W_z/W_o/d = 8/4.5/1 \mu\text{m}$ )

	Physical Meaning	1-VCSEL; Series	3-VCSELS; Series	1-VCSEL; Parallel	2-VCSELS; Parallel
$R_{\text{pad}}(\text{total})$	Pad Resistance ( $\Omega$ )	9	27	6	3
$L_{\text{pad}}(\text{total})$	Pad Inductance (pH)	150	310	135	87
$C_p(\text{total})$	Parasitic Capacitance (fF)	67	17	67	124
$R_c(\text{total})$	Contact Resistance ( $\Omega$ )	80	380	85	37
$C_o$	Oxide layer Capacitance (fF)	65	65	65	65
$R_a$	Diffusion Resistance ( $\Omega$ )	13	100	18	15

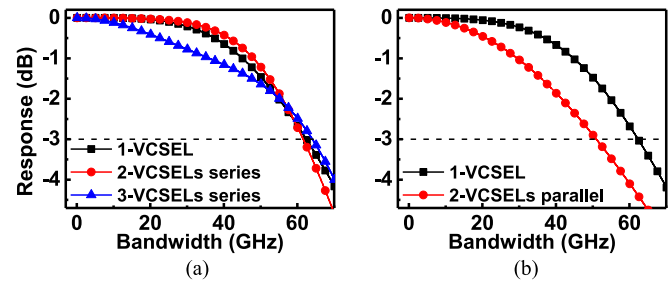


Fig. 14. (a) Extracted RC-limited frequency responses of the (a) series array ( $W_z/W_o/d = 8/3.5/1 \mu\text{m}$ ) and (b) parallel array ( $W_z/W_o/d = 8/4.5/1 \mu\text{m}$ ).

capacitance of the oxide-relief aperture in each single device;  $R_a$  is the diffusion resistance across the active layers of each single device;  $C_p(\text{total})$ ,  $R_{\text{pad}}(\text{total})$ , and  $L_p(\text{total})$  are the total parasitic capacitance, resistance, and inductance induced by the interconnected metal lines in the array, respectively. By using similar approaches, we can also build an equivalent circuit model for the parallel array. Fig. 13 shows the measured/fitted  $S_{11}$  parameters plotted on a Smith Chart for the parallel and series arrays and the single reference device. Clearly, there is a good match between the measured and fitted  $S_{11}$  traces, from near dc to 30 GHz. The values of the circuit elements used for the fitting process are specified in Table I. The RC-limited frequency response of the single unit reference device, and the two-unit and three-unit parallel and series array structures are extracted using the established equivalent-circuit-model and modeling results. Fig. 14(a) and (b) show the results for the series and parallel arrays. We can clearly see an RC-limited bandwidth for our VCSEL structures fabricated with Zn-diffusion and oxide-relief structures

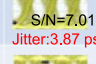
Single Device	BTB	100m	Series 2 devices	BTB	Series 3 devices	BTB	
6mA 32Gb/s 0.46mW	 S/N=3.89	6mA 32Gb/s 0.25mW	 S/N=1.67	5mA 32Gb/s 0.81mW	 S/N=2.14	4mA 32Gb/s 1.22mW	 S/N=7.02 Jitter:4.28 ps
7mA 32Gb/s 0.52mW	 S/N=4.54 Jitter:2.89 ps	7mA 32Gb/s 0.27mW	 S/N=3.25	7mA 32Gb/s 0.89mW	 S/N=7.15	5mA 32Gb/s 1.41mW	 S/N=7.30 Jitter:3.71 ps
8mA 32Gb/s 0.58mW	 S/N=5.46 Jitter:2.77 ps	8mA 32Gb/s 0.28mW	 S/N=3.35	9mA 32Gb/s 0.94mW	 S/N=7.42	6mA 32Gb/s 1.52mW	 S/N=7.01 Jitter:3.87 ps
						7mA 32Gb/s 1.54mW	 S/N=6.89 Jitter:4.16 ps

Fig. 15. Measured 32 Gbit/sec transmission results through 2 (BTB) and 100 meter OM4 MMF using the single unit reference device and series VCSEL array under different bias currents ( $W_z/W_o/d = 8/3.5/1 \mu\text{m}$ ).

Single Device	BTB	100m	Parallel 2 devices	BTB	100m		
6mA 32Gb/s 0.56mW	 S/N=5.53	4 mA 32Gb/s 0.19mW	 S/N=2.97	10mA 32Gb/s 0.92mW	 S/N=4.68	9mA 32Gb/s 0.34 mW	 S/N=4.33
7mA 32Gb/s 0.67mW	 S/N=6.95 Jitter:2.84 ps	6mA 32Gb/s 0.28mW	 S/N=6.04	12mA 32Gb/s 1.11mW	 S/N=7.20	10mA 32Gb/s 0.40mW	 S/N=5.59 Jitter:4.01 ps
8mA 32Gb/s 0.73mW	 S/N=7.48 Jitter:2.61 ps	8mA 32Gb/s 0.36mW	 S/N=6.64	14mA 32Gb/s 1.25mW	 S/N=7.92	12mA 32Gb/s 0.44mW	 S/N=7.84 Jitter:2.73 ps
				16mA 32Gb/s 1.31mW	 S/N=8.61	15mA 32Gb/s 0.52mW	 S/N=9.12 Jitter:2.64 ps
				18mA 32Gb/s 1.4mW	 S/N=8.68		 Jitter:2.18 ps

Fig. 16. Measured 32 Gbit/sec transmission results through 2 (BTB) and 100 meter OM4 MMFs using the single unit reference device and parallel VCSEL array under different bias currents ( $W_z/W_o/d = 8/4.5/1 \mu\text{m}$ ).

(to reduce the differential resistance and parasitic capacitance, respectively), the RC-limited bandwidth ( $f_{RC}$ ) in excess of 60 GHz, much larger than the measured E-O 3-dB bandwidth ( $\sim 25$  GHz), as shown in Figs. 7 and 8. This indicates that the major factor limiting the bandwidth in our VCSEL unit is the internal response time rather than the external  $f_{RC}$ . The degradation in the RC and net E-O bandwidths for a parallel/series array structure based on this VCSEL unit can thus be minimized. As can be clearly seen in Fig. 14(b), the RC-limited bandwidth for even a 2-VCSEL parallel array can be as high as 50 GHz, which is still far above the net E-O bandwidth ( $\sim 25$  GHz). This result indicates that the unique Zn-diffusion/oxide-relief apertures can greatly relax the trade-off between the speed (RC-limited bandwidth) and output power performance in high-power VCSEL arrays [12]. Such devices should have important applications in optical wireless communications and infrared light projectors for high-speed sensing [22].

Figs. 15 and 16 show the 32 Gbit/sec transmission results for the series and parallel arrays, respectively. In each figure, the results for transmission through back-to-back (BTB; 2 meter OM4 fibers) and 100 meter OM4 fiber for the single unit reference and the arrays are given for comparison. During the transmission experiment, a high-speed 40 Gbit/sec photoreceiver module (R40-850; VI-system)<sup>1</sup>, comprised of a p-i-n photodiode and limiting

Single Device	Parallel 2 devices	Series 2 devices	Series 3 devices
8mA 32Gb/s 0.39mW	 S/N=3.17	14mA 32Gb/s 0.37mW	 S/N=4.68
		7mA 32Gb/s 0.387mW	 S/N=7.02 Jitter:4.28 ps
		7mA 32Gb/s 0.39mW	 S/N=7.30 Jitter:3.71 ps
			 S/N=7.01 Jitter:3.87 ps
			 S/N=6.89 Jitter:4.16 ps

Fig. 17. Measured 32 Gbit/sec eye-patterns through the 100 meter OM4 MMF for the single unit reference device ( $W_z/W_o/d = 8/4.5/1 \mu\text{m}$ ), parallel ( $W_z/W_o/d = 8/4.5/1 \mu\text{m}$ ), and series VCSEL arrays ( $W_z/W_o/d = 8/3.5/1 \mu\text{m}$ ) under the same optical power at the receiving-end (around 0.4 mW).

amplifier with a 30 GHz 3-dB optical-to-electrical bandwidth for the whole module, is used. A 32 Gbit/s non-return-to-zero (NRZ) electrical signal with a pseudo-random binary sequence (PRBS) length of  $2^{15}-1$  is generated through a pattern generator. All devices are tested under the same peak-to-peak driving voltage (0.45 V) and the optimized bias current to evaluate the quality of the eye patterns. The values of timing jitter in each eye pattern, which have clear eye-opening performance, are specified. As can be seen in Fig. 15, although the series array has a higher slope efficiency, larger output power at the receiving-end, and faster modulation speed than does the single unit reference device, they have larger values of timing jitter in their BTB eye-patterns. Furthermore, this phenomenon will become more serious as the number of units in the series array increases, which would make error-free 32 Gbit/sec transmission through a 100 meter OM4 fiber with our series array infeasible. Such serious jitter can be attributed to the significant microwave reflections between the  $50 \Omega$  signal source and high internal impedance ( $>200 \Omega$ ) of the series array itself, as illustrated in Figs. 2 and 10.

On the other hand, as shown in Fig. 16, with a bias current around twice that of the single reference device, the two-unit parallel array not only has a larger signal-to-noise (S/N) ratio but also less timing jitter with 32 Gbit/sec eye patterns for both BTB and 100 meter OM4 transmission. There are two possible reasons for the superior transmission performance of the parallel array compared to the single unit device. One is the higher output power and the other is the lower impedance mismatch (between the device and the signal source) induced by microwave reflections and timing jitter, as noted in Fig. 11. In order to figure out which of these is the dominant factor, we installed an additional optical attenuator along the fiber channel to control the optical power at the receiving-end for a fair comparison of the transmission performance.

Fig. 17 shows the transmission results through the 100 meter OM4 fiber for the single unit reference device, two-unit parallel device, and two-unit and three-unit series devices. The optical power at the receiving-end of each measurement is fixed at 0.38 mW. We can clearly see that the two-unit parallel device exhibits the best 32 Gbit/sec transmission performance. Fig. 18 shows the transmission results of the single unit device and two-unit parallel arrays through a 2 meter OM4 fiber (BTB) at the maximum data rate for error-free performance. A higher data rate for transmission (48 vs. 44 Gbit/sec) with less timing jitter is obtained for the two-unit parallel array than for the single unit device. These measurement results clearly indicate the good

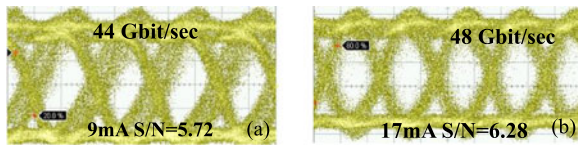


Fig. 18. Measured eye patterns with maximum error-free data rates through a 2 meter OM4 MMF (BTB) for the (a) single unit reference device (44 Gbit/sec) and (b) two-unit parallel array (48 Gbit/sec) ( $W_z/W_o/d = 8/4.5/1 \mu\text{m}$ )

impedance match between the VCSEL and the driving circuit which can greatly improve the frequency response of the total MMF channel and maximum transmission data rate.

#### IV. CONCLUSION

In conclusion, the trade-off between the RC-limited bandwidth and output power performance can be greatly relaxed through the use of Zn-diffusion and oxide-relief apertures in series or parallel VCSEL arrays. For example in the three-unit series, a three-fold improvement in the maximum output power is obtained without sacrificing the 3-dB O-E bandwidth ( $\sim 25$  GHz) as compared to that of the single unit reference device. In addition, the Zn-diffusion apertures can manipulate the optical far-field patterns of the array and minimize the coupling loss with a standard OM4 MMF. Although the series array exhibits superior static and dynamic performance to the single reference unit, its measured BTB eye-patterns show larger values of timing jitter. On the other hand, the two-unit parallel array exhibits the best high-speed transmission performance, which includes a smaller timing jitter, a larger S/N ratio of eye-pattern, and the highest maximum data rate (48 Gbit/sec) through an OM4 MMF, among the proposed series array structures and the single VCSEL. This is because the parallel array provides a device impedance close to the  $50 \Omega$  signal source and thus minimizes the timing jitter induced by microwave reflections. Overall, our proposed VCSEL array structure has good potential for applications in high-speed (50 Gbit/sec) MMF and optical wireless linking.

#### REFERENCES

- [1] P. Moser, P. Wolf, G. Larisch, H. Li, J. A. Lott, and D. Bimberg, "Energy-efficient oxide-confined high-speed VCSELs for optical interconnects," in *Proc. SPIE*, vol. 9001, Feb. 2014, Art. no. 900103.
- [2] D. M. Kuchta *et al.*, "A 50 Gb/s NRZ modulated 850 nm VCSEL transmitter operating error free to 90 °C," *J. Lightw. Technol.*, vol. 33, no. 4, pp. 802–810, Feb. 2015.
- [3] E. Haglund *et al.*, "30 GHz bandwidth 850 nm VCSEL with sub-100 fJ/bit energy dissipation at 25–50 Gbit/s," *Electron. Lett.*, vol. 51, no. 14, pp. 1096–1098, Jul. 2015.
- [4] D. M. Kuchta *et al.*, "A 71-Gb/s NRZ modulated 850-nm VCSEL-based optical link," *IEEE Photon. Technol. Lett.*, vol. 27, no. 6, pp. 577–580, Mar. 2015.
- [5] K.-L. Chi *et al.*, "Single-mode 850 nm VCSELs for 54 Gbit/sec on-off keying transmission over 1 km multi-mode fiber," *IEEE Photon. Technol. Lett.*, vol. 28, no. 12, pp. 1367–1370, Jun. 2016.
- [6] K. Szczerba *et al.*, "4-PAM for high-speed short-range optical communications," *J. Opt. Commun. Netw.*, vol. 4, pp. 885–894, Nov. 2012.
- [7] I-Cheng Lu *et al.*, "Very high bit-rate distance product using high-power single-mode 850 nm VCSEL with discrete multi-tone modulation formats through OM4 multi-mode fiber," *IEEE J. Sel. Topics Quantum Electron.*, vol. 21, no. 6, Nov./Dec. 2015, Art. no. 1701009.

- [8] R. Puerta *et al.*, "107.5 Gb/s 850 nm multi- and single-mode VCSEL transmission over 10 and 100 m of multi-mode fiber," in *Proc. Opt. Fiber Commun. Conf. Exhib.*, Anaheim, CA, USA, Mar. 2016, Paper Th5B.5.
- [9] I. Cheng Lu *et al.*, "Ultra low power VCSEL for 35-Gbps 500-m OM4 MMF transmission employing FFE/DFE equalization for optical interconnects," in *Proc. Opt. Fiber Commun. Conf. Exhib. Nat. Fiber Opt. Eng. Conf.*, Anaheim, CA, USA, Mar. 2013, Paper JTh2A.75.
- [10] P. Westbergh *et al.*, "High-speed 850 nm VCSELs with 28 GHz modulation bandwidth operating error-free up to 44 Gbit/s," *Electron. Lett.*, vol. 48, no. 18, pp. 1145–1147, Aug. 2012.
- [11] K.-L. Chi *et al.*, "Strong wavelength detuning of 850 nm vertical-cavity surface-emitting lasers for high-speed (>40 Gbit/sec) and low-energy consumption operation," *IEEE J. Sel. Topics Quantum Electron.*, vol. 21, no. 6, Nov./Dec. 2015, Art. no. 1701510.
- [12] R. Safaiani, J. R. Joseph, and K. L. Lear, "Scalable high-CW-power high-speed 980-nm VCSEL arrays," *IEEE J. Quantum Electron.*, vol. 46, no. 11, pp. 1590–1596, Nov. 2010.
- [13] J. T. Getty, E. J. Skogen, L. A. Johansson, and L. A. Coldren, "CW operation of 1.55- $\mu\text{m}$  bipolar cascade laser with record differential efficiency, low threshold, and 50- matching," *IEEE Photon. Tech. Lett.*, vol. 15, no. 11, pp. 1513–1515, Nov. 2003.
- [14] P. Modh, S. Galt, J. Gustavsson, S. Jacobsson, and A. Larsson, "Linear cascade VCSEL arrays with high differential efficiency and low differential resistance," *IEEE Photon. Technol. Lett.*, vol. 18, no. 1, pp. 283–285, Jan. 2006.
- [15] J.-W. Shi, H.-W. Huang, F.-M. Kuo, J.-K. Sheu, W.-C. Lai, and M. L. Lee, "Very-high temperature (200 °C) and high-speed operation of cascade GaN based green light emitting diodes with an InGaIn insertion layer," *IEEE Photon. Technol. Lett.*, vol. 22, no. 14, pp. 1033–1035, Jul. 2010.
- [16] P. Westbergh, J. S. Gustavsson, and A. Larsson, "VCSEL arrays for multicore fiber interconnects with an aggregate capacity of 240 Gb/s," *IEEE Photon. Technol. Lett.*, vol. 27, no. 3, pp. 296–299, Feb. 2015.
- [17] S.-Y. Hu, J. Ko, and L. A. Coldren, "High-performance densely packed vertical-cavity photonic integrated emitter arrays for direct-coupled WDM Applications," *IEEE Photon. Technol. Lett.*, vol. 10, no. 6, pp. 766–768, Jun. 1998.
- [18] M. G. Peters *et al.*, "Band-gap engineered digital alloy interfaces for lower resistance vertical-cavity surface-emitting lasers," *Appl. Phys. Lett.*, vol. 63, pp. 3411–3413, Dec. 1993.
- [19] Y. J. Yang, T. G. Dziura, T. Bardin, S. C. Wang, and R. Fernandez, "Continuous wave single transverse mode vertical-cavity surface-emitting lasers fabricated by helium implantation and zinc diffusion," *Electron. Lett.*, vol. 28, no. 3, pp. 274–276, Jan. 1992.
- [20] J.-W. Shi *et al.*, "Single-mode, high-speed, and high-power vertical-cavity surface-emitting lasers at 850 nm for short to medium reach (2 km) optical interconnects," *J. Lightw. Technol.*, vol. 31, no. 24, pp. 4037–4044, Dec. 2013.
- [21] J.-W. Shi, C.-C. Chen, Y.-S. Wu, S.-H. Guol, and Y.-J. Yang, "High-power and high-speed Zn-diffusion single fundamental-mode vertical-cavity surface-emitting lasers at 850nm wavelength," *IEEE Photon. Technol. Lett.*, vol. 20, no. 13, pp. 1121–1123, Jul. 2008.
- [22] H. Moench *et al.*, "VCSEL based sensors for distance and velocity," in *Proc. SPIE*, vol. 9766, Feb. 2016, Art. no. 97660A.

**Jia-Liang Yen** was born in Kaohsiung, Taiwan, on September 20, 1969. He received the M. S. degree and the Ph.D. degree in electrical engineering from the National Taiwan University, Taipei, Taiwan, in 1998 and 2004, respectively. He is currently an Assistant Professor in the Department of Information Technology, Takming University of Science and Technology, Taiwan. His research interest focuses on the design of high-speed VCSEL

**Xin-Nan Chen**, biography not available at the time of publication.

**Kai-Lun Chi** was born in New Taipei City, Taiwan, on February 10, 1988. He is currently working toward th Ph.D. degree in the Department of Electrical Engineering, National Central University, Taoyuan, Taiwan. His current research interest includes high-speed VCSELs and LEDs for optical interconnect applications.

**Jason (Jyehong) Chen** received the B.S. and M.S. degrees in electrical engineering from the National Taiwan University, Taiwan, in 1988 and 1990, respectively, and the Ph.D. degree in electrical engineering and computer science from the University of Maryland Baltimore County, Baltimore, MA, USA, in 1998. He joined JDSU in 1998 as a Senior Engineer and obtained ten U.S. patents in 2 years. He joined the faculty of the National Chiao-Tung University, Taiwan, 2003, where he is currently a Professor in the Institute of Electro-Optical Engineering and Department of Photonics. He has published more than 100 papers in international journals and conferences. His research interests include hybrid access networks, long reach passive optical networks, and optical interconnects.

**Jin-Wei Shi** (M'03–SM'12) was born in Kaohsiung, Taiwan, on January 22, 1976. In 2003, he joined the Department of Electrical Engineering, National Central University, Taoyuan, Taiwan, where he has been a Professor since 2011. In 2011, 2012, and 2016, he joined the Department of ECE, University of California, Santa Barbara, as a Visiting Professor. His current research interests include ultra-high speed/power photodetectors, THz photonic transmitters, and VCSELs. He has authored or coauthored more than 4 book chapters, 120 Journal papers, 180 conference papers, and holds 30 patents. He received 2010 Da-You Wu Memorial Award.